Check for updates

Time-lapsed nanoscale maps of the elastic modulus of collagen during cross-linking by bimodal AFM†

Clara Garcia-Sacristan and Ricardo Garcia [ID] *

Collagen is the most abundant structural protein in mammals. Collagen in tissues is exposed to cross-linking processes such as glycation which might cause progressive tissue stiffening. Tissue stiffening might be considered a landmark of aging. Yet a quantitative characterization of the elastic modulus of collagen nanofibers under different cross-linking processes and stages is not available. Bimodal AFM was applied to generate time-lapsed maps of Young's modulus of type I collagen nanoribbons under two cross-linking processes associated, respectively, with the presence of ribose and glutaraldehyde in the solution. Elastic modulus maps were acquired for different incubation times (0, 30 min, 12 h, 24 h and 1 week). The experiments were performed in liquid. The Young's modulus showed an initial sharp increase after an incubation time of 30 min, from a few MPa (native) to 100 MPa. From then onwards we measured a monotonic increase until a saturation value of about 2 GPa was reached after one week. We did not observe a dependence on the elastic modulus evolution using ribose *versus* glutaraldehyde. The saturation value was very similar to that measured on dry collagen nanoribbons.

Introduction

Collagen is the most abundant structural protein and the main component in the extracellular matrix (ECM). It can be found in all tissues, such as tendons, cartilage, bone and cornea.[1–4] Collagen's mechanical properties are crucial for its correct function.[5–9] Its strength and elasticity play a role in all connective tissues. However, these mechanical properties can be affected by the aging process.[10–13]

Cross-linking processes, and in particular glycation, are a key factor in the stiffening and aging of tissues. Collagen fibrils are naturally exposed to glycation due to their exposure to exogenous sugars. The glycation process in collagen follows the Maillard reaction mechanism. This glycation is a non-enzymatic, multi-step chemical reaction between protein's free amino-groups and reducing sugars. This chemical reaction produces Advanced Glycation End-products (AGEs). The accumulation of AGEs is responsible for premature tissue stiffness.[14–16]

Ribose and glutaraldehyde are molecules that might induce cross-linking processes in collagen fibrils. Ribose is an exogenous reducing sugar that participates in the biological aging

process and the formation of AGEs.[15,18] Glutaraldehyde is a very common material in tissue engineering.[14,18,19]

Several studies have measured the elastic modulus of collagen (uncrosslinked) under near-physiological and non-physiological conditions (air).[5,8,10–13,17–20,27–34] Baldwin *et al.* applied the AFM force-volume to quantify the effects of tendon overload on the structure of individual collagen fibrils.[8] The age-related stiffness of collagen has been studied by measuring the mechanical properties of glycated collagen scaffolds. Yang *et al.* used AFM to determine the Young's modulus of glutaraldehyde cross-linked collagen fibrils under tensile strength.[17] Vaez *et al.* reported that the elastic modulus of collagen fibrils decreased as a function of glycation, whereas the elastic modulus of collagen scaffolds increased.[21] Sloseris and Forde quantified how AGEs affected collagen flexibility by measuring the end-to-end distance of collagen nanoribbons from AFM images.[19]

Here we report time-lapsed and high-spatial resolution elastic modulus maps of the cross-linking steps of collagen nanoribbons by incubating them with ribose (glycation) or glutaraldehyde. AGEs are the result of the reaction of collagen with reducing sugar, but other reactive molecules might also participate as cross-linkers in the aging process.[14]

The high-spatial resolution elastic modulus maps were generated by bimodal AFM.[10,22–26,35] Bimodal AFM is characterized by its quantitative accuracy, high spatial resolution and fast data acquisition which make it possible to obtain nanomechanical mapping of unstable intermediate species of collagen

Instituto de Ciencia de Materiales de Madrid, CSIC, c/ Sor Juana Inés de la Cruz 3, 28049 Madrid, Spain. E-mail: r.garcia@csic.es

glycation. We mapped the time-lapsed elastic modulus of every step of the Maillard reaction, at incubation times of 0 s, 30 min, 12 h, 24 h and 1 week with a spatial resolution in the sub-10 nm range (2 nm per pixel). We revealed the gradual increase in the elastic modulus along the evolution of the reaction, reaching a saturation value after one week of incubation time. The presence of AGEs was confirmed from fluorescence measurements. We obtained a similar trend and elastic modulus values using glutaraldehyde as the cross-linking agent.

We compared the elastic modulus of collagen nanoribbons in physiological solution and under cross-linking processes with that obtained in an air (dry) environment. We observed that the elastic modulus values of collagens after one week of incubation in buffer were very similar to those measured in air.

Results and discussion

Fig. 1a shows a scheme of the bimodal AFM setup. Bimodal AFM is based on the simultaneous excitation of two eigen-

modes, in this case the first and second eigenmodes. The bimodal configuration used in the experiments is amplitude modulation-open loop (AM-OL) where the values of the amplitudes A_1, A_2, and the phase shifts ϕ_i are used to determine the sample's elastic modulus (Fig. 1a). The free amplitudes (A_{01}, A_{02}) were selected prior to the experiments. From these observables, the elastic (Young's) modulus E is obtained directly using the following equation:[10]

$$E = \sqrt{\frac{8}{RA_1}} \frac{2Q_1A_1}{k_1A_{01}\cos\phi_1} \left(\frac{k_2A_{02}\cos\phi_2}{2Q_2A_2}\right)^2 \qquad (1)$$

where R is the tip's radius and Q_i is the quality factor.

However, the above expression is only valid for a semi-infinite sample and should not be used to determine the elastic modulus of finite-thickness collagen nanoribbons. An appropriate elastic modulus of the collagen nanoribbons (thickness 4–5 nm) is obtained using bottom-effect corrections.[36,37] These corrections are needed to remove the influence of the rigid support (mica) on the apparent elastic modulus of the
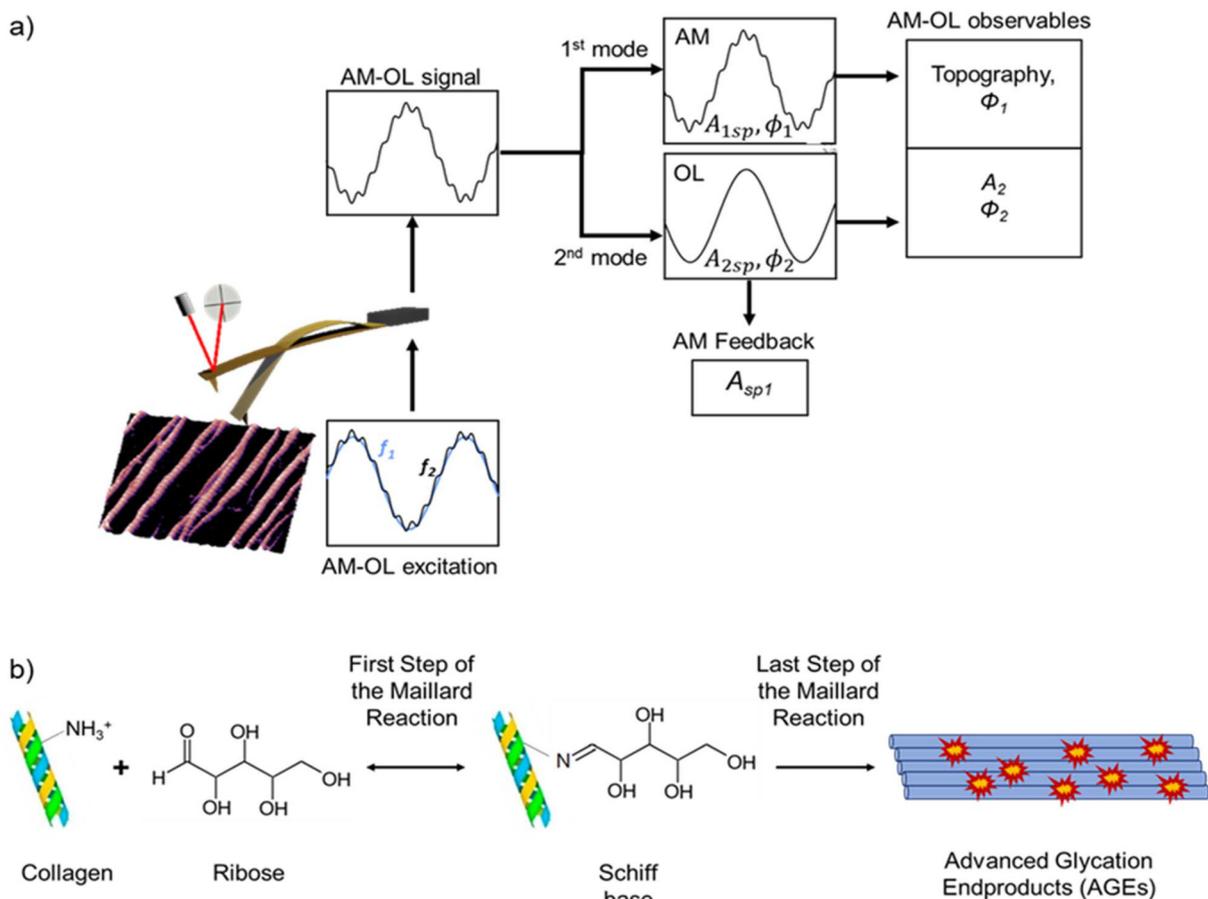

Fig. 1 Schemes of the bimodal AFM configuration and the Maillard reaction mechanism. (a) Bimodal AFM (AM–OL configuration) showing the excitation and detection signals and the observables. (b) In the Maillard reaction the amino groups of collagen molecules react with the aldehyde groups of the ribose. The first step of the Maillard reaction is the formation of an intermediate species, the Schiff base. The formation of the advanced glycation end-products (AGEs) in the nanoribbon is the last step of the reaction.

much softer collagen molecules (Materials and methods). Muscovite mica (~50 GPa) was used as the solid support.

Low force values were required to image soft samples and avoid their deformation. To minimize the collagen damage during nanomechanical mapping, the measurements were performed by applying forces in the 0.2–2.5 nN range. Forces cannot be measured directly while imaging in amplitude modulation or bimodal AFM modes. The forces were determined using a dynamic AFM simulator (dForce 2.0).[38]

Nanomechanical properties during collagen glycation

The Maillard reaction describes the mechanism for the glycation of collagen (Fig. 1b). In the first step, the aldehyde group of the reducing sugar reacts with the amino groups of the collagen molecule. For our experiments the sugar used was ribose. The amino groups taking part in the reaction belong to the lysine and arginine amino acids. This first step in the reaction produces the formation of a Schiff base. The Schiff base is an intermediate species in the reaction which is not stable. The last step in the Maillard reaction is the formation of advanced glycation end products (AGEs) which are irreversibly bonded to the collagen molecules.[14,15] The reaction was performed under physiological conditions of pH and at a temperature of 27 °C.

In the case of using glutaraldehyde as a crosslinker, the reaction is similar to the Maillard mechanism. This particular reaction is also a non-enzymatic, multi-step chemical reaction between protein's free amino-groups and the aldehyde groups of glutaraldehyde.[14] The first step also involves the formation of a Schiff base followed by a rearrangement of molecules and resulting in the corresponding end-products.

Fig. 2 shows the time-lapsed (30 min, 12 h, 24 h and 1 week) nanomechanical maps of the stages in collagen glycation with ribose (top panels). The cross-sections along the dashed lines marked in the nanomechanical maps are shown in the bottom panels. For an incubation time of 30 min, the image was captured 30 min after incubation and approximately 15 min after the mica sample was immersed in solution. The 15 min delay from immersion to imaging accounted for the time required to approach and position the sample under the tip, and to start the imaging process. The measurement parameters and tip calibration were completed prior to this. The same procedure was followed for all other incubation times, with images taken approximately 15 min after the specified incubation period.

Fig. 2a shows the elastic map of collagen after 30 minutes of incubation with ribose which corresponds to the first stage in the Maillard reaction, that is, the formation of the Schiff base. The cross-section shows a variation of the elastic modulus from 80 ± 7 MPa (gap region) to 130 ± 10 MPa (overlap region). The variation of the elastic modulus possesses a periodicity of 67 nm matching the D-band periodicity. These values are one order of magnitude higher than that measured on the same sample under native conditions, that is, before the presence of ribose. Fig. 2b shows the nanomechanical map of ribose glycated collagen after twelve hours of incubation. The average elastic modulus is 1.0 ± 0.2 GPa. This value is about one order of magnitude higher than that found at 30 min and two orders of magnitude higher than that found for native collagen nanoribbons. In this stage of the reaction (30 min), we were not able to observe the D-band periodicity. This finding suggested that collagen undergoes a rearrange-
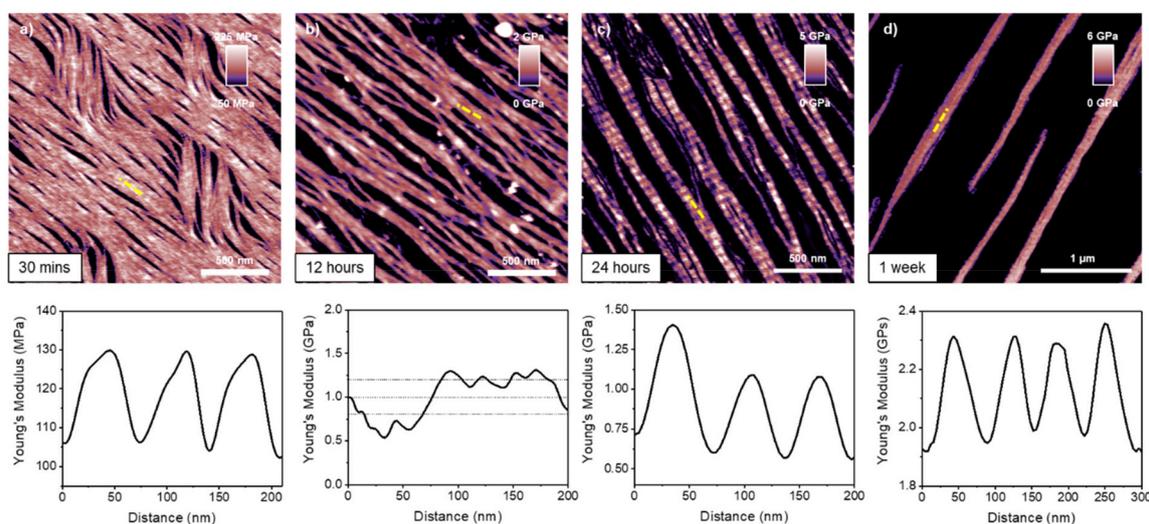

Fig. 2 Time-lapsed elastic modulus maps of the collagen nanoribbons during its glycation with ribose and their cross-sections (marked lines in yellow). (a) Elastic modulus maps of collagen resulting from an incubation time of 30 min. (b) Elastic modulus maps of collagen resulting from an incubation time of 12 h. (c) Elastic modulus maps of collagen resulting from an incubation time of 24 h. (d) Elastic modulus maps of collagen resulting from an incubation time of 1 week. The maps were obtained in buffer by applying a peak force on the nanoribbons of 5.2 nN (25 nN on mica). Additional bimodal AFM data: $f_1 = 586$ kHz, $k_1 = 0.16$ nN nm^{-1}, $Q_1 = 1.5$; $f_2 = 3303$ kHz, $k_2 = 7.9$ nN nm^{-1}, $Q = 6.8$; $A_{01} = 15$ nm, and $A_{02} = 0.1$ nm. The cross-section profiles were obtained from a single nanoribbon by averaging 10 neighbouring profiles of the same length.

ment process in the nanoribbon internal structure. Lysine and arginine residues are among the amino acids responsible for the electrostatic interaction between collagen molecules that causes the corresponding assembly and formation of the D-band pattern.[39] Here the lysine and arginine residues take part in the glycation which might interfere with the internal electrostatic interaction and the structure conformation.[16,39–42] After 24 hours of incubation (Fig. 2c) the rearrangement is complete and the structure of the D-band is again observed. The cross-section shows a variation of the elastic modulus from 0.65 ± 0.07 GPa (gap region) to 1.1 ± 0.2 GPa (overlap region). For longer incubation times (1 week) of the average elastic modulus, we observed an increase in the gap, 2.00 ± 0.06 GPa, and an increase in the overlap region, 2.27 ± 0.05 GPa (Fig. 2d). The d-band periodicity is still present but the density of nanoribbons decreases. The decrease in nanoribbon density can be attributed to the glycation of lysine and arginine residues. Glycation likely disrupts key intermolecular interactions, thereby impairing the lateral growth and assembly of collagen nanoribbons. Both ribose and glutaraldehyde target lysine and arginine residues, interfering with electrostatic interactions that are essential for proper collagen alignment and self-assembly. As the incubation time increases, the number of crosslinks and advanced glycation end-products (AGEs) increases. This effect is supported by the linear rise in the fluorescence signal over time. After three months of incubation, a significant proportion of lysine and arginine residues were modified, reducing their availability for interactions with neighbouring collagen molecules. This extensive modification hindered further nanoribbon formation. This effect explained the observed decline in nanoribbon density at extended time points.

Nanomechanical properties of cross-linked collagens by glutaraldehyde

Fig. 3 shows the time-lapsed (30 min, 12 h, 24 h, and 1 week) elastic maps of collagen, incubated with a different cross-linker, glutaraldehyde (shown in the top panels). The cross-sections along the dashed lines marked in the nanomechanical maps are shown in the bottom panels. Glutaraldehyde behaves similarly to a reducing sugar. The molecule also possesses the aldehyde group necessary for the reaction to occur. The study of the time-lapsed elastic maps follows the same incubation times performed in the ribose experiments: 30 min, 12 h, 24 h and 1 week. The elastic modulus of 30 min incubated collagen (Fig. 3a), which corresponds with the first stage in the Maillard reaction (the formation of the Schiff base), shows values varying from 50 ± 7 MPa (gap region) to 120 ± 10 MPa (overlap region). These values are one order of magnitude higher than that measured on the same sample under native conditions, that is, before the presence of glutaraldehyde. Fig. 3b shows the elastic maps of the collagen nanoribbons measured after 12 h of glutaraldehyde incubation time. An average elastic modulus of 1.0 ± 0.2 GPa was obtained. This value is about one order of magnitude higher than that found at 30 min and two orders of magnitude higher than that found for native collagen nanoribbons. The D-band periodicity is lost which suggests that in the reaction, the collagen molecules undergo a rearrangement in the nanoribbon internal structure. After 24 hours (Fig. 3c) of incubation time the D-band is recovered. The cross-section shows a variation of the elastic modulus from 0.22 ± 0.09 GPa (gap region) to 1.1 ± 0.2 GPa (overlap region). Fig. 3d shows the collagen nanoribbon's elastic map for a longer incubation time (1 week). We
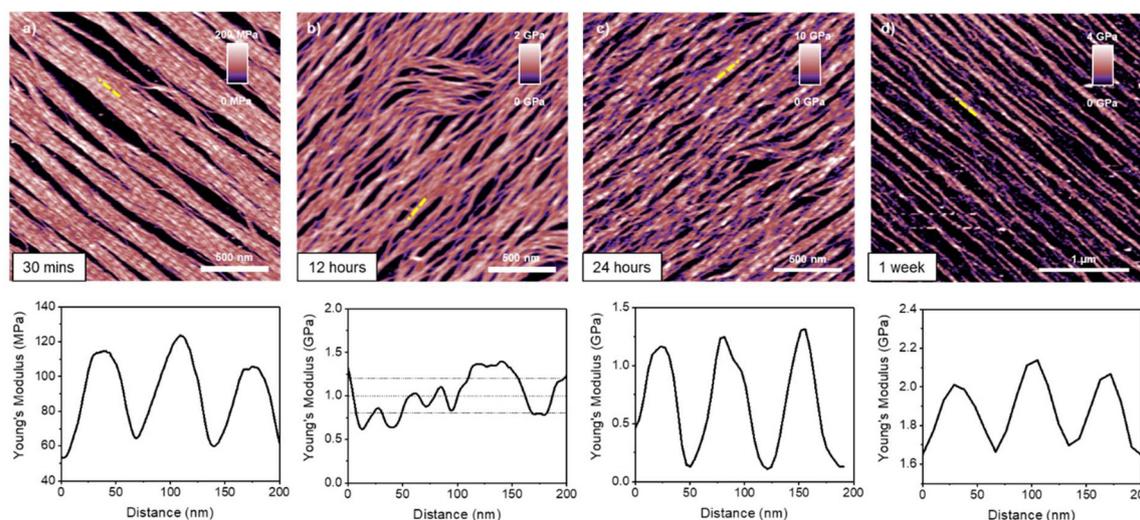

Fig. 3 Time-lapsed elastic modulus maps of the collagen nanoribbons during its crosslinking with glutaraldehyde at incubation times of 30 min (a), 12 h (b), 24 h (c) and 1 week (d) and their cross-sections (marked lines in yellow). The maps were obtained in buffer by applying a peak force on the nanoribbons of 1.3 nN (15 nN on mica). Additional bimodal AFM data: $f_1 = 435$ kHz, $k_1 = 0.15$ nN nm^{-1}, $Q_{11} = 1.5$; $f_2 = 7139$ kHz, $k_2 = 9.84$ nN nm^{-1}, $Q_2 = 3.6$; $A_{01} = 9$ nm, and $A_{02} = 0.45$ nm. The cross-section profiles were obtained from a single nanoribbon by averaging 10 neighbouring profiles of the same length.

observed an increase in the average elastic modulus for the gap, 1.67 ± 0.04 GPa, and the overlap region, 2.0 ± 0.1 GPa. The D-band periodicity is still present but the density of nanoribbons is decreased.

The alignment of collagen nanoribbons arises from the influence of the substrate. The mica lattice dictates the growth direction. The interaction between the amino acid chains and the orientation of the OH groups on the mica surface induced the alignment of the tropocollagen molecules.[10,43,44]

Fig. 4 summarizes the Young's modulus values of the collagen nanoribbons as a function of the incubation time in the presence of either ribose or glutaraldehyde. We observed a significant increase in the elastic modulus for every step in the reaction. Collagen at the start of the reaction (0 s) possesses an elastic modulus below 10 MPa. In the next step a Schiff base is formed which increases collagen's elastic modulus by one order of magnitude (in the 90–100 MPa range). When the incubation time reaches 12 hours, collagen suffers another increase in its elastic modulus, up to 1.0 GPa. In this step of the reaction, there seems to be a rearrangement of its internal structure which might explain the disappearance of the D-band structure. After 24 hours of incubation time, collagen maintains the values of the elastic modulus at 1.1 GPa (overlap region) and 0.22–0.65 GPa (gap region). The formation and accumulation of the AGEs in the collagen nanoribbon is the final step in the reaction. This process increases the stiffness of fibers.

Longer incubation periods were also studied. After one week of incubation, the elastic modulus increased to the 1.8–2.2 GPa range. Remarkably, we also observed that the density of collagen nanoribbons formed over the substrate decreased after one week of incubation. After three months of incubation time, the number of nanoribbons formed on the substrate was even smaller (Fig. S1†). Overall, we concluded that the crosslinking steps associated with the presence of either ribose or glutaraldehyde produce similar changes in the nanomechanical properties of collagen. For the sake of completeness, the elastic modulus values of collagen nanoribbons measured in air (dry collagen) were also included. These values were very similar to those measured on samples with an incubation time of one week.

Time-lapsed fluorescence tracking

The changes in the nanomechanical properties were correlated with changes in the fluorescence signal from the collagen nanoribbons. To confirm the formation of AGEs we performed fluorescence measurements following the one-week incubation time. AGEs have a fluorescence response which might be used to assess their relative level in the collagen nanoribbons.[45–47]

Fig. 5 shows the fluorescence readings of collagen nanoribbons for different incubation times. Fig. 5a shows the fluo-
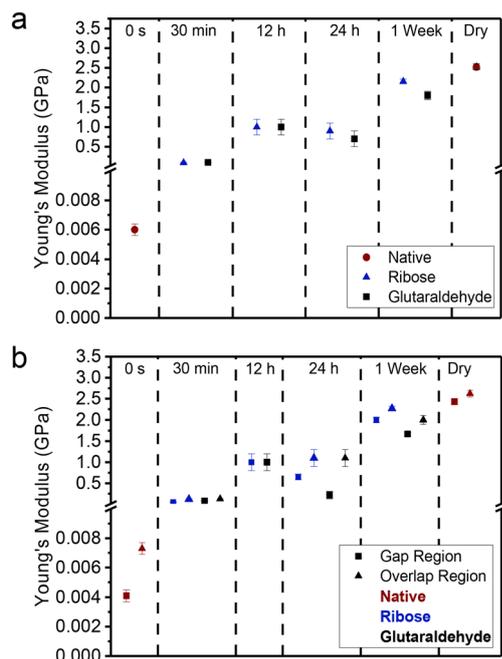

Fig. 4 Elastic modulus of the collagen nanoribbons during glycation (ribose) and crosslinking (glutaraldehyde) processes for incubation times of 0 s, 30 m, 12 h, 24 h and one week. The values are the averages between the elastic modulus of the gap and overlap region of each nanoribbon. (b) Same as (a) by separating the gap and overlap region values. For an incubation time of 12 h we could not resolve the D-band structure (see the main text).
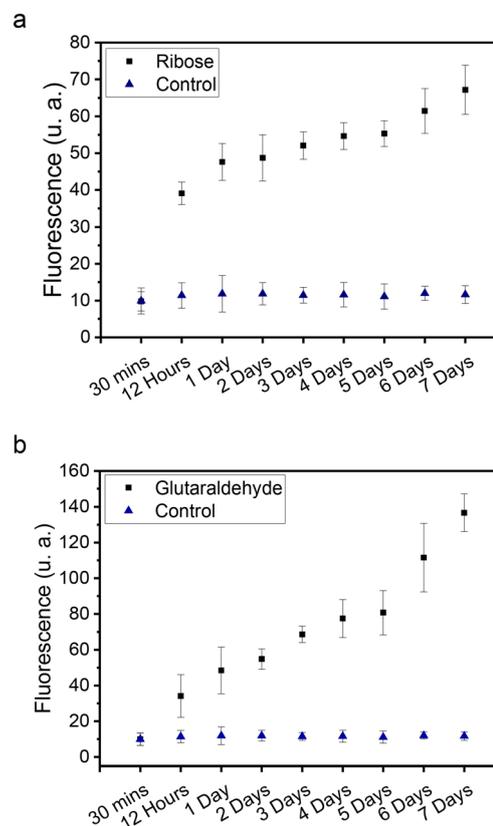

Fig. 5 Fluorescence measurements of collagen nanoribbons for several incubation times. (a) Fluorescence readings of ribose glycated-collagen nanoribbons. (b) Fluorescence readings of glutaraldehyde crosslinked-collagen. Wavelengths of λ_{ex} = 450–490 nm (excitation) and λ_{em} = 500–550 nm (emission).

rescence signal as a function of the incubation time in ribose. The signal associated with the presence of AGEs shows a significant increase with respect to the signal measured on a native collagen nanoribbon sample (control). The emission associated with the AGEs increases from a factor of 40 at 12 hours to a factor of 70 after 7 days. This trend indicates the gradual formation of AGEs. Fig. 5b shows the fluorescence signal as a function of the incubation time in glutaraldehyde. We observed a similar trend. The emission with respect to the control increases from a factor of 30 at 12 hours to a factor of 130 after 7 days. In the case of incubation with glutaraldehyde, the end-products form –N=C–C=C– conjugated double bonds which also exhibit autofluorescence.[48,49] Fig. 5b confirms the gradual increase in the formation of –N=C–C=C– conjugated double bonds, and therefore the gradual formation of the crosslinking end-products.

Conclusions

The Young's modulus values of collagen nanoribbons were measured as a function of the incubation with two crosslinking agents, respectively, ribose and glutaraldehyde. Bimodal AFM allowed us to observe the quantitative mechanical properties of collagen in its crosslinking process. The elastic modulus maps were generated by bimodal AFM. These maps were characterized by a high spatial resolution (2 nm) and a high elastic modulus sensitivity. These features allowed mapping of the nanomechanical properties of collagen during different steps in the Maillard reaction and the final formation of AGEs. The elastic modulus of collagen nanoribbons incubated with ribose increased significantly with the incubation time from a few MPa (native collagen, 0 s) to 100 MPa at 30 min to reach a value of 2.0 GPa (1 week). These values were similar to those obtained in samples of collagen nanoribbons observed in air (dried).

We performed a similar study in collagen nanoribbons incubated with glutaraldehyde. The evolution of the elastic modulus of collagen nanoribbons cross-linked with glutaraldehyde was similar to the trend observed with ribose. The elastic modulus of nanoribbons increased from 10 MPa (native, 0 s) to about 100 MPa (30 min of incubation time) to 2.0 GPa (one week of incubation time).

We noted that the D-band structure disappeared for the incubation time of 12 hours. We hypothesized that this effect might be associated with an internal rearrangement of collagen molecules. The D-band structure was recovered for longer incubation times. However, although the elastic modulus increased, the density of nanofibers formed in the substrate decreased. The elastic modulus maps also show a variation from a GPa range for the dry collagen to less than 10 MPa for the wet collagen. The difference of several orders of magnitude is due to the hydration and swelling of the nanoribbon.

The evolution of the elastic modulus of the collagen was correlated with an increase in the fluorescence emission from the collagen nanoribbons as a function of the incubation time.

Experimental

Collagen preparation

Collagen molecules were obtained from monomeric bovine collagen type I (PureCol, CellSystems GmbH). A phosphate buffer solution PBS was prepared. The as-received PBS (pH = 7.4) contained 0.01 M phosphate, 0.0027 M potassium chloride and 0.137 M sodium chloride. The concentration of KCl was increased to 300 mM to define the standard buffer in the experiments. We added 1 μL of a commercial collagen type I solution (in 0.1 N HCl at pH 2.2) to 1 mL of PBS (pH 7.4). To prepare the crosslinker stock solution, we dissolved glutaraldehyde (ribose) in Milli-Q water to obtain a 100 mM stock solution. Then we added 10 μL of the 100 mM glutaraldehyde (ribose) stock solution to 1 mL of collagen in PBS. The process yielded a final crosslinker concentration of approximately 1 mM in the reaction mixture. D-(−)-Ribose (98%) and glutaraldehyde (50 wt%) were purchased from Sigma-Aldrich.

Measurements were performed with several incubation times: 0 s, 30 min, 12 h, 24 h and 1 week. The incubation was performed at 8 °C. The imaging buffer consisted of PBS (Sigma-Aldrich) with 300 mM KCl (Sigma-Aldrich), pH 7.4 in a solution volume of 200 ml.

Fluorescence measurements

For the fluorescence measurements, the collagen solution was prepared under the same conditions (incubation temperature 8 °C) and concentration (3.0 μg ml^{-1}) as before. The solutions were then added to a Petri dish for measuring. Fluorescence microscopy was performed using an illuminating system built into an optical microscope (HBO 100 lamp, Zeiss, Germany). Wavelengths of λ_{ex} = 450–490 nm (excitation) and λ_{em} = 500–550 nm (emission) were used to monitor the collagen crosslinking process.

Bimodal AFM parameters and measurements

Bimodal-AFM measurements were performed with a Cypher VRS (Oxford Instruments, USA). Bimodal-AFM was operated in air and liquid in the amplitude modulation–open loop AFM mode. Mechanical excitation was used to excite the vibration of the cantilever. The in-air experiments were performed with standard cantilevers (PPP-NCH, NanoAndMore, Germany). Typical values of the resonance frequencies, force constants and quality factors were $f_1 \approx 314$ kHz, $k_1 \approx 48$ N m^{-1}, $Q_1 \approx 600$, and $f_2 \approx 1940$ kHz, $k_2 \approx 1844$ N m^{-1}, $Q_2 \approx 660$. Here, f_i, k_i and Q_i are, respectively, the resonance frequency, the force constant and the quality factor of mode i (i = 1, 2). Typical values of the free amplitudes A_0 and set-point A_{sp} amplitudes were, $A_{01} \approx 110$ nm, $A_{sp} \approx (0.7–0.9)A_{01}$, and $A_{02} \approx 1.2$ nm.

For the in-liquid experiments very small cantilevers (7 μm × 2 μm × 80 nm) (USC-F1.2-k0.15, NanoAndMore, Germany) were used. Typical values of the resonance frequencies, force constants and quality factors in liquid were $f_1 \approx 520$ kHz, $k_1 \approx 0.15$ N m^{-1}, $Q_1 \approx 1.5$, and $f_2 \approx 3303$ kHz, $k_2 \approx 7.9$ N m^{-1} and $Q_2 \approx$ 6.8. Typical values of the free amplitudes A_0 and set-point A_{sp} amplitudes were $A_{01} \approx 10$ nm, $A_{sp1} \approx (0.7–0.9)A_{01}$, and $A_{02} \approx$

0.4 nm. The images were recorded at 2.44 Hz with 1024 × 1024 pixels unless otherwise stated.

The force constants of the cantilever's first and second eigen modes were calibrated by following the protocol given in ref. 50.

The native collagen and cross-linked collagen solutions were rapidly injected into a freshly cleaved muscovite mica disk (Grade V-1, Alpha Biotech Ltd) placed inside the fluid cell of the AFM. Imaging was started without further delay. The temperature of the buffer in the cell was 27 °C.

To remove the influence of the substrate stiffness (mica) on Young's modulus of the collagen (bottom-effect), a bottom-effect correction theory was applied. The theory considers that the force measured by AFM can be separated into two components, one arising from the material as it was semi-infinite and a correction factor associated with its finite thickness h.[36]

$$F_{ts} = F_{Hertz}[1 + F_{bec}(a/h)] \quad (2)$$

where a is the contact radius

$$a = \sqrt{R\delta}$$

The bottom-effect correction was performed using the expressions deduced in ref. 39 for a half-sphere of $R = 11$ nm. We assumed an under-formed collagen thickness $h = 4.5$ nm.

$$\delta_{max} = \frac{k_1 A_{01} \cos \phi_1}{Q_1} \frac{Q_2 A_2}{k_2 A_{02} \cos \phi_2} \quad (3)$$

$$V_1 = -\frac{k_1 A_1 A_{01}}{2Q_1} \cos \phi_1 \quad (4)$$

$$E = \frac{\sqrt{\frac{8}{RA_1}} \frac{V_1}{I^2}}{1 + 1.03\left(\frac{\sqrt{RI}}{h}\right) + 1.25\left(\frac{\sqrt{RI}}{h}\right)^2 + 1.14\left(\frac{\sqrt{RI}}{h}\right)^3 + 0.55\left(\frac{\sqrt{RI}}{h}\right)^4} \quad (5)$$

Author contributions

C. G. S.: methodology, investigation, and writing review and editing. R. G.: conceptualization, methodology, investigation, funding acquisition, supervision, and writing review and editing.

Conflicts of interest

There are no conflicts to declare.

Data availability

All relevant data are within the manuscript and its additional files, and in the Zenodo repository (https://doi.org/10.5281/zenodo.15574388).[51]

Acknowledgements

References

1 P. Fratzl, *Collagen: Structure and Mechanics, an Introduction*, Springer US, 2008, pp. 1–13.

2 D. F. Holmes, Y. Lu, T. Starborg and K. E. Kadler, *Curr. Top. Dev. Biol.*, 2018, **130**, 107–142.

3 M. W. Kirkness, K. Lehmann and N. R. Forde, *Curr. Opin. Chem. Biol.*, 2019, **53**, 98–105.

4 B. J. Bielajew, J. C. Hu and K. A. Athanasiou, *Nat. Rev. Mater.*, 2020, **5**, 730–747.

5 J. Kwon and H. Cho, *Nanomanuf. Metrol.*, 2023, **6**, 30.

6 J. Kwon and H. Cho, *Commun. Biol.*, 2022, **5**, 1229.

7 O. G. Andriotis, S. W. Chang, M. Vanleene, P. H. Howarth, D. E. Davies, S. J. Shefelbine, M. J. Buehler and P. J. Thurner, *J. R. Soc., Interface*, 2015, **12**, 20150701.

8 S. J. Baldwin, L. Kreplak and J. M. Lee, *J. Mech. Behav. Biomed. Mater.*, 2016, **60**, 356–366.

9 A. Stylianou, S. V. Kontomaris, C. Grant and E. Alexandratou, *Scanning*, 2019, **2019**, 8452851.

10 V. G. Gisbert, S. Benaglia, M. R. Uhlig, R. Proksch and R. Garcia, *ACS Nano*, 2021, **15**, 1850–1857.

11 P. Panwar, G. Lamour, N. C. W. Mackenzie, H. Yang, F. Ko, H. Li and D. Brömme, *J. Biol. Chem.*, 2015, **290**, 23291–23306.

12 L. Yang, K. O. Van der Werf, C. F. Fitié, M. L. Bennink, P. J. Dijkstra and J. Feijen, *Biophys. J.*, 2008, **94**, 2204–2211.

13 M. J. Buehler, *J. Mech. Behav. Biomed. Mater.*, 2008, **1**, 59–67.

14 K. Adamiak and A. Sionkowska, *Int. J. Biol. Macromol.*, 2020, **161**, 550–560.

15 J. Gaar, R. Naffa and M. Brimble, *Org. Chem. Front.*, 2020, **7**, 2789–2814.

16 M. Rufin, M. Nalbach, M. Rakuš, M. Fuchs, M. Poik, G. Schitter, P. J. Thurner and O. G. Andriotis, *Acta Biomater.*, 2024, **189**, 208–216.

17 L. Yang, K. O. Van der Werf, P. J. Dijkstra, J. Feijen and M. L. Bennink, *J. Mech. Behav. Biomed. Mater.*, 2012, **6**, 148–158.

18 D. Haluszka, S. Aminmansour, P. Tóth, S. Aminmansour and M. Kellermayer, *J. Dent. Res.*, 2022, **101**, 1510–1516.

19 D. Sloseris and N. R. Forde, *Matrix Biol.*, 2025, **135**, 153–160.

20 M. Minary-Jolandan and M. F. Yu, *Biomacromolecules*, 2009, **10**, 2565–2570.

21 M. Vaez, M. Asgari, L. Hirvonen, G. Bakir, E. Khattignavong, M. Ezzo, S. Aguayo, C. M. Schuh, K. Gough and L. Bozec, *Acta Biomater.*, 2023, **155**, 182–198.

22 E. T. Herruzo, A. P. Perrino and R. Garcia, *Nat. Commun.*, 2014, **5**, 3126.

23 M. Kocun, A. Labuda, W. Meinhold, I. Revenko and R. Proksch, *ACS Nano*, 2017, **11**, 10097–10105.

24 S. Benaglia, V. G. Gisbert, A. P. Perrino, C. A. Amo and R. Garcia, *Nat. Protoc.*, 2018, **13**, 2890–2907.

25 S. Benaglia, C. A. Amo and R. Garcia, *Nanoscale*, 2019, **11**, 15289–15297.

26 R. Garcia, *Chem. Soc. Rev.*, 2020, **49**, 5850–5884.

27 G. Giubertoni, L. Feng, K. Klein, G. Giannetti, L. Rutten, Y. Choi, A. Van Der Net, G. Castro-Linares, F. Caporaletti, D. Micha, J. Hunger, A. Deblais, D. Bonn, N. Sommerdijk, A. Šarić, I. M. Ilie, G. H. Koenderink and S. Woutersen, *Proc. Natl. Acad. Sci. U. S. A.*, 2024, **121**, e2313162121.

28 C. A. Amo, A. P. Perrino, A. F. Payam and R. Garcia, *ACS Nano*, 2017, **11**, 8650–8659.

29 S. J. Baldwin, A. S. Quigley, C. Clegg and L. Kreplak, *Biophys. J.*, 2014, **107**, 1794–1801.

30 M. Vassaux, *Biomacromolecules*, 2024, **25**, 4809–4815.

31 M. R. Uhlig and R. Magerle, *Nanoscale*, 2017, **9**, 1244–1256.

32 C. A. Grant, D. J. Brockwell, S. E. Radford and N. H. Thomson, *Appl. Phys. Lett.*, 2008, **92**, 233109.

33 C. A. Grant, D. J. Brockwell, S. E. Radford and N. H. Thomson, *Biophys. J.*, 2009, **97**, 2985–2992.

34 D. M. Arvelo, C. Garcia-Sacristan, E. Chacón, P. Tarazona and R. Garcia, *J. Chem. Phys.*, 2024, **160**, 164701.

35 A. Labuda, M. Kocuń, W. Meinhold, D. Walters and R. Proksch, *Beilstein J. Nanotechnol.*, 2016, **7**, 970–982.

36 P. D. Garcia and R. Garcia, *Biophys. J.*, 2018, **114**, 2923–2932.

37 V. G. Gisbert and R. Garcia, *ACS Nano*, 2021, **15**, 20574–20581.

38 V. G. Gisbert and R. Garcia, *Soft Matter*, 2023, **19**, 5857.

39 S. Bansode, U. Bashtanova, R. Li, J. Clark, K. H. Müller, A. Puszkarska, I. Goldberga, H. H. Chetwood, D. G. Reid, L. J. Colwell, J. N. Skepper, C. M. Shanahan, G. Schitter, P. Mesquida and M. J. Duer, *Sci. Rep.*, 2020, **10**, 3397.

40 V. Mull and L. Kreplak, *Nanoscale Adv.*, 2022, **4**, 4829–4837.

41 P. Mesquida, D. Kohl, O. G. Andriotis, P. J. Thurner, M. Duer, S. Bansode and G. Schitter, *Sci. Rep.*, 2018, **8**, 10126.

42 C. Garcia-Sacristan, V. G. Gisbert, K. Klein, A. Šarić and R. Garcia, *ACS Nano*, 2024, **18**, 18485–18492.

43 W. W. Leow and W. Hwang, *Langmuir*, 2011, **27**, 10907–10913.

44 B. Narayanan, G. H. Gilmer, J. Tao, J. J. De Yoreo and C. V. Ciobanu, *Langmuir*, 2014, **30**, 1343–1350.

45 M. J. Bellmunt, M. Portero, R. Pamplona, M. Muntaner and J. Prat, *Lung*, 1995, **173**, 177–185.

46 D. R. Sell and V. M. Monnier, *J. Biol. Chem.*, 1989, **264**, 21597–21602.

47 B. J. Ortwerth, M. Prabhakaram, R. H. Nagaraj and M. Linetsky, *Photochem. Photobiol.*, 1997, **65**, 666–672.

48 T. Zhang, Z. Yu, Y. Ma, B. S. Chiou, F. Liu and F. Zhong, *Food Hydrocolloids*, 2022, **124**, 107270.

49 Z. Yu, J. Wu, T. Zhang, C. Chen, Y. Ma, H. Liu and J. Li, *Collagen Leather*, 2024, **6**, 29.

50 A. Labuda, M. Kocun, M. Lysy, T. Walsh, J. Meinhold, T. Proksch, W. Meinhold, C. Anderson and R. Proksch, *Rev. Sci. Instrum.*, 2016, **87**, 073705.

51 C. Garcia-Sacristan and R. Garcia, *Zenodo*, 2025, DOI: **10.5281/zenodo.15574388**.